

A Koopman operator approach for the vertical stabilization of an off-road vehicle

Jake Buzhardt* Phanindra Tallapragada*

* *Department of Mechanical Engineering, Clemson University, Clemson, SC 29634 USA (e-mail: jbzhar@g.clemson.edu, ptallap@clemson.edu).*

Abstract: Vehicles traversing off-road terrains experience modes of dynamics that are not usually encountered on-road. Deformable terrains with significant variations in height and the presence of bumps can lead to significant vertical dynamics in a vehicle. Besides rider discomfort and safety of the vehicle, in the case of unmanned vehicles, these vertical dynamics coupled with pitch motion can produce significant disturbances to sensors such as cameras. Reducing these vertical dynamics is therefore important. However any control design for this problem has to first contend with the modeling complexity of vehicle-tire-terrain interaction. Motivated by recent developments in dynamical systems, we propose the use of the Koopman operator to obtain a linear representation for both the vehicle and terrain interaction dynamics as well as the effect of the control input. As a test case for this framework we address the problem of stabilizing the vertical dynamics of a half-car model moving on a deformable terrain using a propulsive force on the car as the sole control input. The terramechanics are modeled using the Bekker-Wong equations. Using the Koopman operator framework, we obtain a lifted, linear representation of the nonlinear control system, which is then used to formulate the optimal control problem as a constrained linear quadratic model predictive control problem on the lifted system. The framework proposed in this paper can potentially be extended to design a combination of data-driven and physics-based control algorithms for intelligent suspensions, motion control and path-tracking for unmanned ground vehicles on unstructured terrains.

Keywords: Vehicle dynamic systems, Motion control, Model Predictive Control, Koopman operator.

1. INTRODUCTION

In many military applications, unmanned ground vehicles (UGVs) must navigate smoothly and efficiently over uneven, deformable terrain. The vertical dynamics of a vehicle can be significant while traversing such terrain. The vertical and pitching modes of motion can couple in an unsafe manner endangering the vehicle. Besides safety concerns, the vertical dynamics of the vehicle manifest as disturbances for onboard sensors like cameras, lidar and IMUs and can lead to deteriorated autonomous performance. The usual approach to minimizing the vertical oscillations of a vehicle in the case of on road driving over small bumps is to control the parameters of the vehicle suspension system Elbanhawi et al. (2015); Fialho and Balas (2000); Fu and Dong (2021); Yu et al. (2021). The off-road environment however presents several serious challenges: the terrain is not rigid, it is usually more uneven, terrain conditions can change more due to precipitation, and most importantly there do not exist well defined lanes or roads. Besides the control of the suspension parameters, control

of the speed of the vehicle itself can become an important means to reduce the vertical dynamics of a vehicle. This is unlike the case of on-road driving where the speed of a vehicle is determined to a great extent by traffic conditions and legal speed limits.

Controlling the speed of an off-road UGV with the goal of minimizing vertical oscillations requires at least low degree of freedom vehicle models that incorporate important physics of terrain-tire interaction. Even simplified models like the half-car or the bicycle when coupled with a model of a deformable terrain lead to governing equations that are nonlinear differential equations with many terrain parameters and forces that have to be calculated by surface integrals along the tires, as discussed for instance in Ishigami et al. (2007); Taheri et al. (2015); Dallas et al. (2021). While previous works have addressed some problems on path tracking on deformable terrain, the vehicle models usually ignore the vertical dynamics. This essentially is equivalent to assuming that the normal reaction transmitted by the wheels to the ground is just the weight of the vehicle, a constant, thus simplifying the governing equations. This assumption is no longer valid when the vertical dynamics of a vehicle due to the suspension are present or when the curvature of the terrain to be traversed is high. To overcome the challenges of the complex physics, a more suitable representation of the governing model

* This work was supported by the Automotive Research Center (ARC), a US Army Center of Excellence for modeling and simulation of ground vehicles, under Cooperative Agreement W56HZV-19-2-0001 with the US Army DEVCOM Ground Vehicle Systems Center (GVSC).

**DISTRIBUTION A. Approved for public release; distribution unlimited. OPSEC #6307

that is also simultaneously amenable to standard control systems tools is desirable.

Recent progress on data driven methods to model dynamical systems using the Koopman operator can be valuable for this purpose. Essentially the Koopman operator acts linearly on a ‘lifted’ space of functions that is associated with the observables of the dynamical system, see for instance Lasota and Mackey (1994); Budišić et al. (2012) for a review. Projecting the space of observables to a finite but high dimensional space leads to a linear but high dimensional dynamical system. This approach has proven fruitful to obtain reduced order linear models and identification of main modes of in fluid flows, see for example Rowley et al. (2009); Schmid (2010); Li et al. (2017). More recent progress has been made on extending the Koopman operator method to a control system, see for example Korda and Mezić (2018); Kaiser et al. (2017, 2020); Otto and Rowley (2021). In particular Korda and Mezić (2018) proposes an approach to formulate a high dimensional linear control system that is amenable to model predictive control (MPC). This enables the formulation high dimensional constrained linear optimal control problems. This approach is well-suited for the problem of controlling the dynamics of off-road vehicles as it generates a convenient linear representation for both the complex governing dynamics as well as the control input.

The application of the Koopman operator method to problems in vehicle dynamics is novel and the results in this paper suggest that more complex control problems, including control of suspension parameters, path tracking problems with higher degree of freedom vehicle models can be addressed in a systematic computational framework.

2. SYSTEM MODELLING

The vehicle system considered in this work is modelled by a half-car model to represent the vehicle’s vertical dynamics with the Bekker-Wong terramechanics model (see Wong and Reece (1967); Ishigami et al. (2007) for more details) used to describe friction forces arising from the wheel-terrain interaction. The governing equations of these models are given in the following subsections.

2.1 Half-car vehicle model

The vertical and pitching dynamics of the vehicle are described by a half-car model, a single-track vehicle model which approximates the suspension dynamics by a linear spring and damper at both the front and rear axle. A schematic of this model is shown in Fig. 1. The governing equations for the half-car model are

$$m\ddot{z} = -k_r(z_r - z_{rg}) - c_r(\dot{z}_r - \dot{z}_{rg}) - k_f(z_f - z_{fg}) - c_f(\dot{z}_f - \dot{z}_{fg}) \quad (1)$$

$$I_y\ddot{\theta} = (k_r(z_r - z_{rg})l_r + c_r(\dot{z}_r - \dot{z}_{rg})l_r - k_f(z_f - z_{fg})l_f - c_f(\dot{z}_f - \dot{z}_{fg})l_f) \cos \theta \quad (2)$$

where k_f, k_r, c_f, c_r are the stiffness and damping values at the front and rear suspensions, respectively; and l_f, l_r are the distances from the front and rear axle to the vehicle’s center of mass. The variables z_f and z_r are the vertical displacements of the vehicle chassis from equilibrium at the front and rear axle, given by

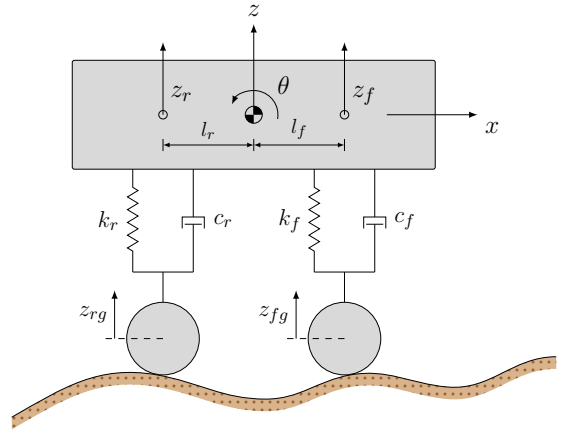


Fig. 1. Schematic of half-car vehicle model

$$z_f = z + l_f \sin \theta \quad , \quad z_r = z - l_r \sin \theta. \quad (3)$$

Similarly, the variables z_{fg} and z_{rg} represent the vertical displacement in the suspension due to the terrain at the front and rear wheels. These are directly related to the wheel sinkage, h , and the terrain profile, which is represented as a function of the longitudinal distance, $H(x)$. So, we have

$$z_g = H(x) - h \quad , \quad (4)$$

which is evaluated at both the front and rear wheels. The computation of the wheel sinkage is discussed further in Sec. 2.2.

In order to compute the wheel forces from the terrain model, normal load N at each wheel must be computed. From the half-car model, this is computed as

$$N_i = \frac{1}{2}mg - k(z_i - z_{gi}) - c(\dot{z}_i - \dot{z}_{gi}) + m_w\ddot{H} \quad (5)$$

where $i \in \{r, f\}$, m_w is the mass of the wheel, and

$$\ddot{H} = \frac{d^2 H}{dx^2} \dot{x}^2 + \frac{dH}{dx} \ddot{x}$$

is the vertical acceleration of the wheel.

The longitudinal motion of the vehicle is described by a sum of forces in the x direction to give

$$m\ddot{x} = F_{xf} + F_{xr} + F_u \quad (6)$$

where F_{xf} and F_{xr} are wheel forces derived from the Bekker-Wong terramechanics model and F_u is an additional tractive/braking force, considered as a control input.

2.2 Terramechanics Model

In order to compute the forces F_{xf} and F_{xr} at the wheel resulting from the terrain interactions, a Bekker-based terramechanics model is implemented. With such, the forces are computed by integrating the normal and shear stress distributions over the contact region between the wheel and terrain. The normal and shear stress distributions σ and τ_x are taken to be functions of the sinkage h , which, in turn, is assumed to be a function of the contact angle ϑ . These are given by

$$\sigma(\vartheta) = \left(\frac{k_c}{b} + k_\phi \right) h(\vartheta)^n \quad (7)$$

$$\tau_x(\vartheta) = (c + \sigma(\vartheta) \tan \phi) \left(1 - e^{-j_x/k_x} \right) \quad (8)$$

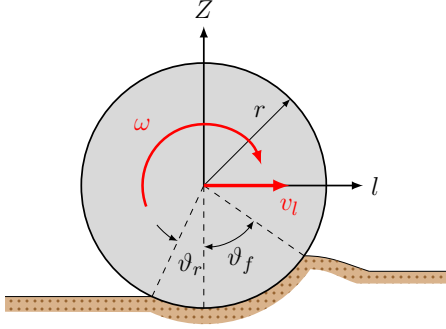


Fig. 2. Schematic of wheel-terrain interaction model

where k_c , k_ϕ , and n are terrain parameters, b is the effective width of the wheel, and the sinkage h is given as follows.

$$h(\vartheta) = \begin{cases} r(\cos \vartheta - \cos \vartheta_f) & \vartheta_m \leq \vartheta \leq \vartheta_f \\ r(\cos \vartheta_e - \cos \vartheta_f) & \vartheta_r \leq \vartheta \leq \vartheta_m \end{cases}$$

Here ϑ_f and ϑ_r are the front and rear contact angles as depicted in Fig. 2, and ϑ_m is the angle of maximum normal stress. These can be computed as

$$\vartheta_f = \cos^{-1} \left(1 - \frac{h_f}{r} \right) \quad (9)$$

$$\vartheta_m = (a_0 + a_1 s) \vartheta_f \quad (10)$$

$$\vartheta_r = (b_0 + b_1 s) \vartheta_f \quad (11)$$

$$\vartheta_e = \vartheta_f - \left(\frac{\vartheta - \vartheta_r}{\vartheta_m - \vartheta_r} \right) (\vartheta_f - \vartheta_m) \quad (12)$$

where a_0 , a_1 , b_0 , b_1 are soil-dependent parameters. For the shear stress $\tau_x(\vartheta)$, the shear displacement $j_x(\vartheta)$ is also needed. This is given by

$$j_x(\vartheta) = r[(\vartheta_f - \vartheta) - (1 - s)(\sin \vartheta_f - \sin \vartheta)] \quad (13)$$

where $s = (r\omega - v_l)/r\omega$ is the slip ratio. Since wheel rotation ω is not tracked as a state in our simulations, the slip ratio s is assumed to maintain a constant value.

With this, $\sigma(\vartheta)$ and $\tau_x(\vartheta)$ are fully defined with the exception of the maximum sinkage h . These distributions can then be integrated to yield the longitudinal and normal forces on the wheel as

$$F_x = \int_{\vartheta_r}^{\vartheta_f} rb(\tau_x(\vartheta) \cos \vartheta - \sigma(\vartheta) \sin \vartheta) d\vartheta \quad (14)$$

$$F_z = \int_{\vartheta_r}^{\vartheta_f} rb(\tau_x(\vartheta) \sin \vartheta + \sigma(\vartheta) \cos \vartheta) d\vartheta \quad (15)$$

Finally, the maximum sinkage h_f can be found by applying the boundary condition that the resultant force in the vertical direction is equal to the normal reaction. In this work, h_f is found using Eq. 15 as the zero of the expression $F_z - N = 0$ through a Newton-Raphson iterative procedure. Once h_f is found, the stress distributions are fully defined and Eqs. 14 can be used to compute the longitudinal force on the wheel.

3. KOOPMAN LIFTING

Koopman-based methods for MPC have received significant attention in recent years (see, for example Korda and Mezić (2018); Peitz et al. (2020); Folkestad and Burdick

(2021)), as MPC methods can solve the optimal control problem efficiently online, while satisfying constraints on the states and controls. In this paper, we take the approach of Korda and Mezić (2018), which modifies the extended dynamic mode decomposition (EDMD) algorithm Williams et al. (2015) to account for the effects of actuation on the system dynamics. More recent works Peitz et al. (2020); Folkestad and Burdick (2021) have shown that a similar data-driven approach can be used to obtain a continuous time, bilinear representation of the system based on the Koopman generator, which can then be implemented for control in a receding horizon manner. While this method appears to be more data efficient Peitz et al. (2020), the resulting system is bilinear and thus the optimal control problem must be solved either by using nonlinear optimization methods Peitz et al. (2020); Folkestad and Burdick (2021) or by quantizing the control input and reducing the problem to selecting a control from a pre-defined set on each step, as suggested by Peitz et al. (2020); Klus et al. (2020). In addition, these methods also require that data on the derivatives of the states either be measured or computed by finite differencing, while the discrete-time approach only requires information about the states. For these reasons, we opt for the alternative approach of Korda and Mezić (2018), which gives a linear representation of the system and thus a convex formulation of the optimal control problem.

The following subsections briefly outline the approach, beginning with a description of the EDMD method for uncontrolled systems in Sec. 3.1 and the extension to actuated systems in Sec. 3.2.

3.1 Koopman operator for uncontrolled systems

The Koopman operator (Lasota and Mackey (1994) or Budišić et al. (2012)) is an infinite dimensional linear operator which propagates observable functions of the states forward in time under the dynamics of the system. That is, for the dynamical system

$$x_{t+1} = F(x_t) \quad (16)$$

where $x_t \in \mathbb{X} \subset \mathbb{R}^n$ and $F : \mathbb{X} \mapsto \mathbb{X}$ the action of the Koopman operator $\mathcal{K} : \mathcal{L}^\infty(\mathbb{X}) \mapsto \mathcal{L}^\infty(\mathbb{X})$ on an observable function $g : \mathbb{X} \mapsto \mathbb{R}$ is given as follows.

$$\mathcal{K}g(x_t) = (g \circ F)(x_t) = g(x_{t+1}) \quad (17)$$

To approximate the infinite dimensional operator \mathcal{K} , we take the EDMD approach as proposed in Williams et al. (2015), by projecting the observable function g onto the space spanned by a set, \mathbb{D} , of dictionary functions.

$$\mathbb{D} = \{\psi_1, \psi_2, \dots, \psi_k\} \quad (18)$$

That is, we make the approximation

$$\mathcal{K}g(x_t) \approx \mathcal{K}(c^\top \Psi)(x_t) \approx c^\top K^\top \Psi(x_t) \quad (19)$$

where $\Psi : \mathbb{X} \mapsto \mathbb{R}^k$ is a column-vector valued function where the elements are given by $[\Psi(x)]_i = \psi_i(x)$, $c \in \mathbb{R}^k$ is a column vector of coefficients, and $K \in \mathbb{R}^{k \times k}$ is the projection of Koopman operator onto the space of functions spanned by the dictionary \mathbb{D} .

To compute the matrix approximation K of the Koopman operator from data, we gather and store data in the form of snapshot matrices

$$X = [x_1, \dots, x_m] \quad (20)$$

$$Y = [y_1, \dots, y_m] \quad (21)$$

where the matrices X and Y contain m state observations on the columns and where $y_i = F(x_i)$ for $i = 1, \dots, m$. We then lift the measurement data by evaluating the dictionary functions at each measurement to obtain the lifted data matrices $\Psi_X, \Psi_Y \in \mathbb{R}^{k \times m}$ as follows.

$$\Psi_X = [\Psi(x_1), \dots, \Psi(x_m)] \quad (22)$$

$$\Psi_Y = [\Psi(y_1), \dots, \Psi(y_m)] \quad (23)$$

Then, following from Eqs. 17 and 19, we have

$$\Psi_Y = K^\top \Psi_X \quad (24)$$

With this, K can be computed by the following least-squares minimization

$$\min_K \|\Psi_Y \Psi_X^\top - K^\top \Psi_X \Psi_X^\top\|_2^2 \quad (25)$$

where the least squares problem has been written in normal form so that the minimization only depends on the number of dictionary functions used in the projection, not on the number of measurements.

3.2 Controlled systems

For a control system of the form

$$x_{t+1} = F_u(x_t, u_t) \quad (26)$$

where $u_t \in \mathbb{U} \subset \mathbb{R}^p$ is the control input and $F_u : \mathbb{X} \times \mathbb{U} \mapsto \mathbb{X}$, we take a similar approach to obtain a linear representation of the system in a lifted space. That is, we seek a linear approximation of the form

$$\Psi(x_{t+1}) = A\Psi(x_t) + Bu_t \quad (27)$$

where $A \in \mathbb{R}^{k \times k}$ and $B \in \mathbb{R}^{k \times p}$ are linear predictors computed from observed trajectory data. To obtain such an approximation from data, we gather data in the form of snapshot matrices

$$X = [x_1, \dots, x_m] \quad (28)$$

$$Y = [y_1, \dots, y_m] \quad (29)$$

$$U = [u_1, \dots, u_m] \quad (30)$$

as before, where we now have m state observations with $y_i = F_u(x_i, u_i)$ for $i = 1, \dots, m$. We then lift the X and Y data as in Eqs. 22 and 23 and perform the minimization

$$\min_{A, B} \|\Psi_Y - A\Psi_X - BU\|_2^2 \quad (31)$$

or as a least squares problem,

$$\min_M \|V - MW\|_2^2 \quad (32)$$

where

$$W = \begin{bmatrix} \Psi_X \\ U \end{bmatrix} \begin{bmatrix} \Psi_X \\ U \end{bmatrix}^\top, \quad V = \Psi_Y \begin{bmatrix} \Psi_X \\ U \end{bmatrix}^\top,$$

A is given by the first k columns of M , and B is given by the final p columns of $M \in \mathbb{R}^{k \times (k+p)}$.

4. MPC FORMULATION

For the off-road vehicle system as described in Sec 2, the equations of motion define a dynamical system of the form of Eq. 26. With this system, we wish to determine a control strategy for traversing an uneven terrain while reducing vertical oscillations of the vehicle chassis. Such a control problem is readily framed as an optimal control problem,

where these goals are encoded in a cost function. In particular, a receding horizon approach such as MPC allows us to efficiently solve this optimal control problem while accounting for constraints, especially since the Koopman lifting framework allows us to represent the system in a linear fashion. The linear representation of the system is significant, as it ensures that the optimization problem will be convex so long as the objective function is quadratic in the lifted states and controls.

For convenience, we will introduce the notation $z_t = \Psi(x_t)$ for the lifted state, and thus Eq. 27 becomes

$$z_{t+1} = Az_t + Bu_t$$

where A and B are computed as described in Sec. 3.2. With this, we will consider a finite time optimal control problem in terms of the lifted state in the form

$$\min_{u_t, \dots, u_{(t+N-1)}} J((z_j)_{j=t}^{t+N}, (u_j)_{j=t}^{t+N-1}) \quad (33)$$

to be solved at each time step t for the optimal control sequence over an N -step horizon, where the cost function J is given in the form

$$J = (y_N - Cz_N)^\top Q_N (y_N - Cz_N) + \sum_{j=0}^{N-1} \left[(y_j - Cz_j)^\top Q (y_j - Cz_j) + u_j^\top R u_j \right] \quad (34)$$

where the y_j are vector-valued output quantities to be tracked and C is the matrix which relates those outputs to the lifted state. With this formulation, any observable that can be expressed as a linear combination of the lifted states can be expressed in the regulation problem.

5. APPLICATION TO OFF-ROAD VEHICLE PROBLEM

5.1 Data collection

In order to apply the Koopman MPC framework to the off-road navigation problem, we begin by gathering trajectory data by simulating the model described in Sec. 2 of the half-car moving over uneven deformable terrain. The simulations are carried out in MATLAB where the data is gathered at sampling rate of 10 Hz. The model is integrated using MATLAB's built-in variable step, variable order ODE solver, `ode113` between these discrete sampled times.

In all of the simulations performed here, the vehicle parameters are chosen to be representative of a Polaris M-RZR [Polaris Government & Defense (2022)] and the terrain parameters are taken to be representative values of clay Wong and Reece (1967).

For the computation of the Koopman operator, data is gathered from 230 trajectories with randomized initial conditions, integrated over a 20 second timespan (200 samples per trajectory) for 46,000 total measurements. In this data gathering process, the control force F_u is chosen randomly at each timestep and held constant over the 0.1s sampling period. The force is chosen from a uniform distribution on the interval $[-2m, 3m]$, where m is the vehicle mass. The terrain profile used in these simulations is specified as a function of x as $H(x) = 0.04 \sin(0.75x)$.

5.2 Lifting and Operator Computation

Once the trajectory data is generated by running the simulations as described in Sec. 5.1, this data is stored in snapshot matrices as in Eqs. 28-30. The stored states are the longitudinal and vertical position, velocity, and acceleration, as well as the pitch and pitch velocity. That is, the measurement vector is

$$[x, \dot{x}, \ddot{x}, z, \dot{z}, \ddot{z}, \theta, \dot{\theta}]^\top.$$

To carry out the lifting of these states, as in Eq. 22-23, the dictionary functions are chosen to be all monomials in the measured states of up to order 3, as well as the same monomials multiplied by $\cos \theta$ and by $\sin \theta$, for a total of 495 dictionary functions.

With the lifted states, the operators A and B are computed by solving the least squares problem in Eq. 32. For this computation, the matrix W is scaled to improve conditioning and the minimization is performed using MATLAB's built-in generalized minimum residual (`gmres`) routine.

5.3 MPC Implementation

Once the operators A and B are computed, they are used in an MPC implementation, as described in Sec 4. For this, we consider the following optimization problem at each time step

$$\min_{u_t, \dots, u_{(t+N-1)}} \sum_{j=t}^{t+N-1} [q_x(x_j - x_d)^2 + q_z \ddot{z}_j^2 + r u_j^2] \quad (35a)$$

$$\text{subject to: } \Psi(x_{j+1}) = A\Psi(x_j) + B u_j \quad (35b)$$

$$u_{\min} \leq u_j \leq u_{\max} \quad (35c)$$

for $j = t, \dots, t + N - 1$

so that the vertical acceleration \ddot{z} , control effort u , and distance from a desired final position x_d are penalized. This is implemented with a control timestep of 0.1s and a horizon length of $N = 30$ steps (3 s).

With this, two simulations of the MPC implementation are performed and compared in Figs. 3, 4, and 5. In both cases shown, the cost function parameters q_x and r are held constant at 1 and 0.01, respectively; and the desired final position is set to $x_d = 30$ m. The two simulations shown compare the cases where the vertical acceleration of the vehicle is not penalized ($q_z = 0$) and where it is penalized heavily ($q_z = 1000$). All values are reported in standard metric units and angle values are given in radians.

Fig. 3 shows the longitudinal position, velocity and acceleration of the vehicle for the two simulations. We see that in the case where $q_z = 0$, the vehicle accelerates by applying a maximum force at the beginning of the trajectory before smoothly slowing the vehicle to zero velocity as it reaches the desired position. In the case where $q_z = 1000$, the vehicle applies a braking pattern as it begins to approach the peaks of the terrain. From Fig. 4, it can be seen that these deceleration events nearly coincide with the peaks of the terrain profile. The resulting effect of this control on the vertical and pitching dynamics is shown in Fig. 5. This shows that the braking pattern chosen by the MPC controller results in a reduction of the magnitude of oscillations in the vertical acceleration \ddot{z} , as well as the

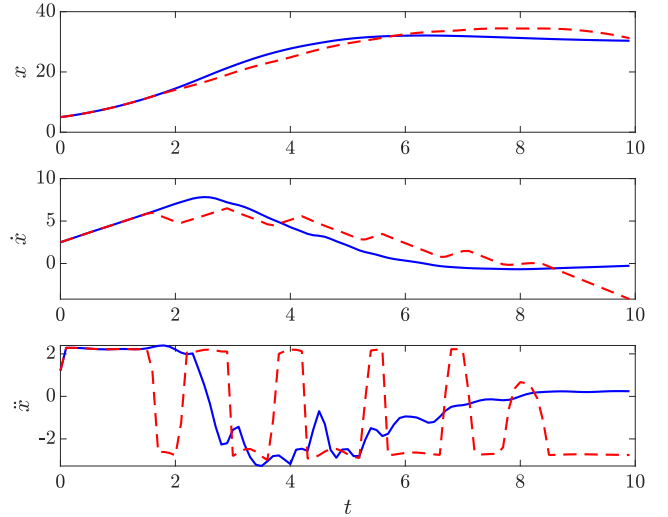


Fig. 3. Longitudinal state trajectories. The lines represent different penalties on vertical acceleration: $q_z = 0$ (—) and $q_z = 1000$ (---), respectively.

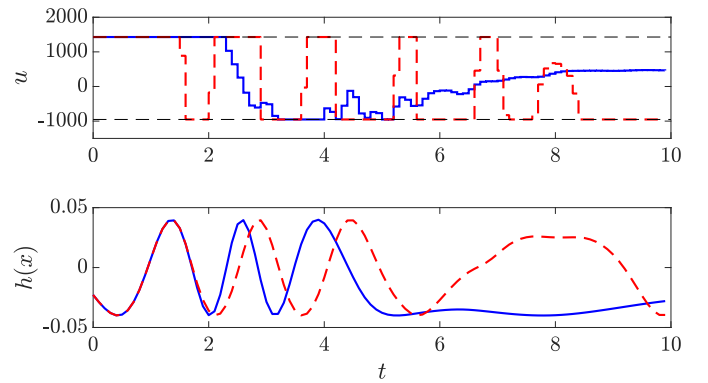


Fig. 4. Top: Longitudinal force control input. Bottom: Terrain elevation experienced by the vehicle. The lines represent different penalties on vertical acceleration: $q_z = 0$ (—) and $q_z = 1000$ (---), respectively. The horizontal black dashed lines show the control constraints, u_{\min} and u_{\max} .

other vertical and pitching states. For example, the RMSE values for the \ddot{z} trajectories shown are 2.595 m/s² and 1.947 m/s² for the $q_z = 0$ and $q_z = 1000$ cases respectively.

6. CONCLUSION

We have shown that through a Koopman-based control strategy, we can identify a high-dimensional, linear representation of an off-road vehicle system moving over an uneven, deformable terrain. With this data-driven representation of the system, we are able to account for the effects of the uneven and deformable terrain and mitigate the unwanted vertical oscillations through a predictive control framework.

Future work could include an extension of this controller to consider preview information about the terrain, which could be obtained from onboard sensors such as cameras or lidar. This information could also be incorporated for controlling additional vehicle features, such as active or semi-active suspensions. Further, in future work, we plan to validate this control scheme in experiment or higher

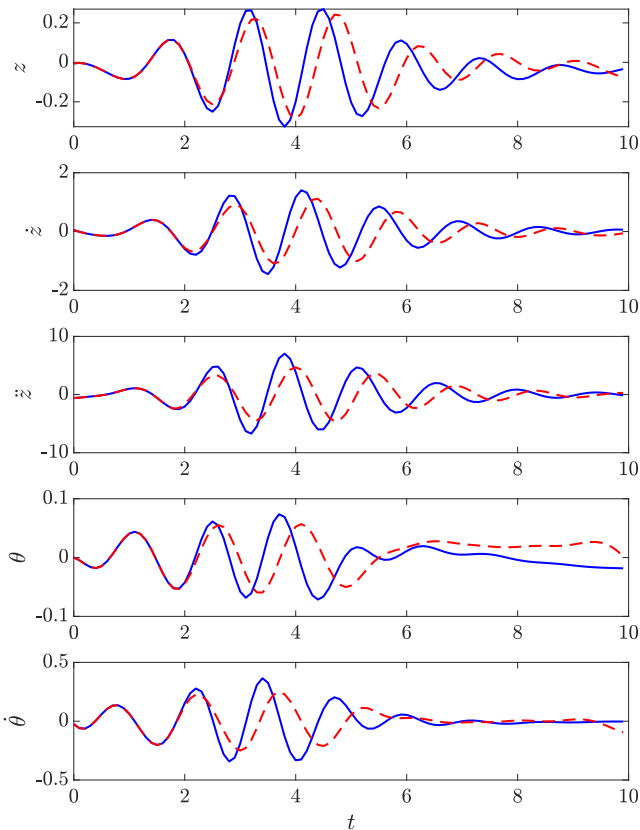


Fig. 5. Vertical and pitching state trajectories. The lines represent different penalties on vertical acceleration: $q_{\ddot{z}} = 0$ (—) and $q_{\ddot{z}} = 1000$ (- - -), respectively.

fidelity simulation as well as extend it to more complex offroad driving scenarios.

REFERENCES

- Budišić, M., Mohr, R., and Mezić, I. (2012). Applied koopmanism. *Chaos: An Interdisciplinary Journal of Nonlinear Science*, 22(4), 047510. doi:10.1063/1.4772195.
- Dallas, J., Cole, M.P., Jayakumar, P., and Ersal, T. (2021). Terrain adaptive trajectory planning and tracking on deformable terrains. *IEEE Transactions on Vehicular Technology*, 1–1. doi:10.1109/TVT.2021.3114088.
- Elbanhawi, M., Simic, M., and Jazar, R. (2015). In the Passenger Seat: Investigating Ride Comfort Measures in Autonomous Cars. *IEEE Intelligent Transportation Systems Magazine*, 7(3), 4–17.
- Fialho, I.J. and Balas, G.J. (2000). Design of nonlinear controllers for active vehicle suspensions using parameter-varying control synthesis. *Vehicle System Dynamics*, 33(5), 351–370.
- Folkestad, C. and Burdick, J.W. (2021). Koopman NMPC: Koopman-based learning and nonlinear model predictive control of control-affine systems. In *2021 IEEE International Conference on Robotics and Automation (ICRA)*, 7350–7356. doi:10.1109/ICRA48506.2021.9562002.
- Fu, Z.J. and Dong, X.Y. (2021). H_∞ optimal control of vehicle active suspension systems in two time scales. *Automatica*, 62(2), 284–292.
- Ishigami, G., Miwa, A., Nagatani, K., and Yoshida, K. (2007). Terramechanics-based model for steering maneuver of planetary exploration rovers on loose soil. *Journal of Field Robotics*, 24(3), 233–250. URL <https://doi.org/10.1002/rob.20187>.
- Kaiser, E., Kutz, J.N., and Brunton, S.L. (2017). Data-driven discovery of Koopman eigenfunctions for control. doi:10.48550/ARXIV.1707.01146. URL <https://arxiv.org/abs/1707.01146>.
- Kaiser, E., Kutz, J.N., and Brunton, S.L. (2020). Data-driven approximations of dynamical systems operators for control. In *The Koopman Operator in Systems and Control*, 197–234. Springer.
- Klus, S., Nüske, F., Peitz, S., Niemann, J.H., Clementi, C., and Schütte, C. (2020). Data-driven approximation of the Koopman generator: Model reduction, system identification, and control. *Physica D: Nonlinear Phenomena*, 406, 132416.
- Korda, M. and Mezić, I. (2018). Linear predictors for nonlinear dynamical systems: Koopman operator meets model predictive control. *Automatica*, 149–160.
- Lasota, A. and Mackey, M.C. (1994). *Chaos, Fractals, and Noise : Stochastic Aspects of Dynamics*. Springer.
- Li, Q., Deitrich, F., Bollt, E.M., and Kevrekidis, I.G. (2017). Extended dynamic mode decomposition with dictionary learning: A data-driven adaptive spectral decomposition of the koopman operator. *Chaos*, 27, 103111.
- Otto, S.E. and Rowley, C.W. (2021). Koopman operators for estimation and control of dynamical systems. *Annual Review of Control, Robotics, and Autonomous Systems*, 4, 59–87.
- Peitz, S., Otto, S.E., and Rowley, C.W. (2020). Data-driven model predictive control using interpolated koopman generators. *SIAM Journal on Applied Dynamical Systems*, 19(3), 2162–2193.
- Polaris Government & Defense (2022). Specs: Polaris mrzr d2 - military tan. URL <https://military.polaris.com/en-us/mrzr-d2-military-tan/specs/>.
- Rowley, C.W., Mezić, I., Bagheri, S., Schlatter, P., and Henningson, D.S. (2009). Spectral analysis of nonlinear flows. *Journal of fluid mechanics*, 641, 115–127.
- Schmid, P.J. (2010). Dynamic mode decomposition of numerical and experimental data. *Journal of fluid mechanics*, 656, 5–28.
- Taheri, Sh., Sandu, C., Taheri, S., Pinto, E., and Gorsich, D. (2015). A technical survey on terramechanics models for tire-terrain interaction used in modeling and simulation of wheeled vehicles. *Journal of Terramechanics*, 57, 1–22.
- Williams, M.O., Kevrekidis, I.G., and Rowley, C.W. (2015). A data-driven approximation of the koopman operator: Extending dynamic mode decomposition. *Journal of Nonlinear Science*, 25(6), 1307–1346.
- Wong, J.Y. and Reece, A. (1967). Prediction of rigid wheel performance based on the analysis of soil-wheel stresses part i. performance of driven rigid wheels. *Journal of Terramechanics*, 4(1), 81–98. URL [https://doi.org/10.1016/0022-4898\(67\)90105-x](https://doi.org/10.1016/0022-4898(67)90105-x).
- Yu, M., Evangelou, S.A., and Dini, D. (2021). Parallel active link suspension: Full car application with frequency-dependent multiobjective control strategies. *IEEE Transactions on Control Systems Technology*, 7, 1–16.